Structural and magnetic properties of the ferroelectric magnet $BaMn_{1-x}Zn_xF_4$, a site diluted square-lattice two-dimensional Heisenberg antiferromagnet with $S=\frac{5}{2}$

J. R. Veira,[1] D. N. Argyriou,[1] K. Kiefer,[1] A. U. B. Wolter,[2,3] D. Alber,[1] M. Meissner,[1] R. Almairac,[4] M. Reehuis,[1] and H. N. Bordallo[1,*]

[1]*Helmholtz-Zentrum Berlin für Materialien und Energie (HZB), Glienicker Strasse 100, D-14109 Berlin, Germany*

[2]*Institut für Physik der Kondensierten Materie, TU Braunschweig, 38106 Braunschweig, Germany*

[3]*Helmholtz-Zentrum Berlin für Materialien und Energie (HZB), c/o BESSY, D-12489 Berlin, Germany*

[4]*Universitè Montpellier II, F-34095 Montpellier Cedex 5, France*

(Received 15 January 2007; revised manuscript received 18 May 2008; published 7 August 2008)

The influence of Zn doping on the structural and magnetic properties of multiferroic $BaMnF_4$ has been investigated using temperature dependent x-ray diffraction and magnetization measurements. With increasing Zn content the transition temperatures of the structural incommensurate phase transition as well as the AF ordering decrease. For $x=0.75$ no incommensurate phase is found anymore. The suppression of the structural transition can be explained due to the smaller size of Zn compared with Mn. The suppression of the antiferromagnetic ordering can be explained by a site dilution of the magnetic structure with nonmagnetic Zn. The percolation threshold is found to be $x_p=0.393(4)$. This is in agreement with predictions for a site-diluted square-lattice weak-anisotropy two-dimensional Heisenberg antiferromagnet with $S=\frac{5}{2}$.

DOI: 10.1103/PhysRevB.78.054104 PACS number(s): 75.30.Kz, 75.47.Lx, 75.80.+q

I. INTRODUCTION

Although materials that exhibit magnetism and ferroelectricity within a single chemical phase have been known for some time,[1] the coupling between these *ferroic* properties has attracted significant recent attention.[2] At the forefront of these new investigations on multiferroic materials are the manganite perovskites such as $RMnO_3$ or RMn_2O_5 as ferroelectricity here arises from inversion symmetric breaking driven by magnetic ordering.[2,3] Mechanisms for such coupling based on exchange striction or the inverse Dzyaloshinskii-Moriya interaction can allow for a strong coupling between ferroelectricity and magnetism such as the flop or the reversal of the ferroelectric polarization with magnetic field.[2]

As magnetoelectric materials are rare it is important to understand the coupling between ferroelectricity and magnetism in as many classes of multiferroics as possible in order to come to a general understanding of the magnetoelectric effect in matter. Another well-known class of magnetic ferroelectrics are the fluorides $BaXF_4$, where X is a transition-metal ion.[4–7] These compounds crystallize with an orthorhombic structure, space group $A2_1am$. As elegantly demonstrated 40 years ago by Eibschutz *et al.*,[8] the first observation of ferroelectricity in an ionic fluoride containing *d*-transition metal ions was made for X=Mn, Fe, Co, Ni, and Zn with a ferroelectric polarization along the *a* direction up to the melting point.[9–14] The X=Fe and Mn compounds are pyroelectric since switching of the ferroelectric polarization has not been demonstrated. This is in part due to the larger ionic radii both ions, which inhibits the ionic displacements responsible for polarization reversal.[8] Furthermore, for X=Mn, Fe, Co, and Ni antiferromagnetic (AF) ordering of X-ion spins is observed with Nèel temperatures T_N of 26, 60, 70, and 80 K, respectively.[9,15]

By choosing to study $BaMn_{1-x}Zn_xF_4$ we aim to control the size of the mean-ionic size of the X ion as well as the strength of the magnetic interactions. The $BaMnF_4$ end member of this solid solution exhibits an incommensurate crystal (IC) structure[16] below $T_{IC}=253$ K, which was found to be of ferroelastic origin.[17] The average crystal structure of the low-temperature phase of $BaMnF_4$ has a monoclinic symmetry[18] and the incommensurate phase has a propagation vector $q=(\epsilon,0.5,0.5)$, $\epsilon=0.39$. The magnetic structure of $BaMnF_4$ can be described to a large degree using a commensurate propagation vector $q_m=(0,0.5,0.5)$. However, as shown by Cox *et al.*,[16] the Mn spins also couple to the IC crystal structure as weak magnetic reflections are also observed below T_N with the same IC wave vector as that found for the crystal structure. At lower temperatures an anomaly in the static dielectric constant along the *a* and *b* axis observed at T_N have tentatively been described in terms of a novel phonon-magnon coupling.[19] In contrast, $BaZnF_4$ has no observable structural transition to an incommensurate phase.[20] However x rays and inelastic neutron-scattering studies indicated an incipient instability into an IC phase that is distinct from the IC phase for the X=Mn end member.[21,22] More recently, from a first-principles study Ederer and Spaldin[4] argued that the origin ferroelectricity in the multiferroic $BaXF_4$ compounds is due to a single unstable polar zone-center phonon triggered solely by size effects, and no charge transfer occurs as a result of the structural distortion.

In this paper we present crystallographic and magnetic measurements on the $BaMn_{1-x}Zn_xF_4$ system. These new structural and magnetic measurements on the solid solution $BaMn_{1-x}Zn_xF_4$ show that the suppression[23,24] of T_{IC} is followed by the suppression of T_N as the Zn content increases. The suppression of T_N follows a percolation model with a percolation threshold $x_p^{exp}=0.393(4)$, in good agreement with the expected behavior for a site-diluted square-lattice two-dimensional (2D) Heisenberg antiferromagnet. Concurrently the suppression of T_{IC} shows a linear decrease with *x*, or the mean radius of the X ion, demonstrating a steric effect on this transition.

TABLE I. Structural refinement of $BaMn_{0.5}Zn_{0.5}F_4$ in the $A2_1am$ space group. The last three lines compare the lattice parameters in $BaMnF_4$, $BaMn_{0.5}Zn_{0.5}F_4$, and $BaZnF_4$. Values for the two end members of the series are reported from Refs. 11 and 20.

Atom	x/a	y/b	z/c	U11	U22	U33	U12
Ba	0.4537	0.34799(9)	0.5	1.3764(495)	2.2677(453)	0.60012(315)	1.0455(439)
Mn or Zn	−0.00992(133)	0.41543(48)	0	1.4002(2934)	1.0714(1855)	1.9577(2293)	0.5455(1891)
F1	0.19345(31)	0.30044(6)	0	1.19205(438)	0.9714(308)	1.8662(415)	0.0654(354)
F2	−0.27936(28)	0.33492(8)	0	1.0786(494)	2.4115(450)	1.3529(390)	−0.4368(455)
F3	0.32887(38)	0.46715(7)	0	1.5557(558)	1.1986(378)	2.5674(559)	−0.5415(372)
F4	0.01115(40)	0.42140(13)	0.5	2.7630(661)	4.8948(937)	0.6753(357)	1.2702(60)
Compound	a(Å)	b(Å)	c(Å)	V(Å^3)			
BaMnF	5.9845(3)	15.098(2)	4.2216(13)	381.438			
$BaMn_{0.5}Zn_{0.5}F_4$	5.9110(6)	14.7886(15)	4.1903(5)	366.297(68)			
$BaZnF_4$	5.8391(8)	14.546(3)	4.1974(6)	356.5			

II. EXPERIMENTAL DETAILS

Single crystals of $BaMn_{1-x}Zn_xF_4$ with $x=0$, 0.1, 0.15, 0.20, 0.30, 0.50, and 0.75 were synthesized by the Bridgman-Stockbarger method. Using neutron activation analysis the nominal Zn content was confirmed for all samples within an error of less than 6% in each case.

The $A2_1am$ crystal structure of all samples was confirmed by x-ray diffraction using a HUBER four-circle goniometer with wavelength $\lambda=0.71073$ Å on single-crystal splints of approximate size 1 mm. More detailed structure analysis at 300 K of $BaMn_{0.5}Zn_{0.5}F_4$ was undertaken using the four-circle single-crystal neutron diffractometer E5 with $\lambda=0.88430$ Å, located at the BENSC Facility at the HZB. In this experiment, 608 independent reflections were measured while the data was analyzed using the program XTAL.[25]

Magnetization measurements were performed on samples of dimensions $2\times1\times0.5$ mm^3 with a vibrating sample magnetometer [VSM, part of a quantum design physical property measurement system (PPMS Model 6000)] and a superconducting quantum interference device (SQUID) magnetometer (quantum design magnetic property measurement system—MPMS XL). The measurements were performed in the temperature range from 1.9 to 300 K. Magnetization measurements on the $BaMn_{0.05}Zn_{0.95}F_4$ and $BaMn_{0.5}Zn_{0.5}F_4$ were obtained on samples oriented along the crystallographic axis using a standard x-ray Laue camera. For all other compositions, only samples with random orientation have been used.

III. EXPERIMENTAL RESULTS

A. Structural investigations

The crystallographic symmetry for $x=0.15$ and 0.5 samples was confirmed using Weissenberg photographs taken at room temperature and at 120 K (see Ref. 24). The systematic absences correspond to $k+l=2n+1$ for general reflections hkl, and to $h=2n+1$ for $h0l$, reproducing the conditions for space group $A2_1am$. A further analysis of the crystal structure of the $x=0.5$ sample was undertaken using a $10\times5\times5$ mm^3 single crystal using the neutron four-circle diffractometer E5 located at BENSC. The crystal was found to be of excellent quality exhibiting resolution limited Bragg reflections and the absence of secondary phases. Analysis of the neutron single-crystal diffraction data was performed using the $A2_1am$ structure. Best fits to the data were obtained for a random distribution of 50% Mn^{2+} and 50% Zn^{2+} on the X ion sites, giving values of $R=0.053$ and $wR=0.039$. As the crystal structure is noncentrosymmetric, the x position of the Ba atoms was arbitrarily fixed during the refinement, so the origin of the unit cell could be defined. The results of the analysis are given in Table I. In the same table we also list lattice constants of three compositions from the crystals we examined.[11,20,23] These values are broadly consistent with the formation of a solid solution of $BaMn_{1-x}Zn_xF_4$. Here the **a** and **b** axis decrease with increasing x due to the greater differences in the average M-F distance of 2.098 Å for M=Mn and 1.95 Å for M=Zn. The behavior along **c** is consistent with the observation of very similar $M-M_i$ distance, of 3.86 and 3.92 Å for Zn and Mn, respectively.[11]

To determine the influence of the Zn doping to the transition temperature T_{IC}, we measured the temperature dependence of the intensity and wave vector of the (2-ϵ 0.5 2.5) super-lattice reflections between 10 and 300 K. The incommensurate modulation was found to be at $\epsilon\sim0.39$; the peak width and the peak position were found to be independent of temperature for $T>T_{IC}$. A typical scan through the IC reflection as a function of temperature measured from our $x=0.1$ crystal is shown in Fig. 1(a). Here the data were measured on warming and it can be seen that the intensity of the superlattice reflections rapidly decreases and the reflections disappears across T_{IC}.

In Fig. 1(b) we show the temperature dependence of the intensity of this IC reflection measured from our $x=0.1$, 0.2, 0.3, and 0.5, crystals. As suggested by the data T_{IC}, as defined by the disappearance of the IC reflection, decreases with increasing x. Here we find that for $x=0.10$ and 0.20, sharp transitions occur at 231 and 195 K, respectively. The small crystal size of the $x=0.30$ sample made measurement of the IC reflection challenging, however, the IC reflection could be followed below $T_{IC}=147$ K, while for the $x=0.50$ crystal we find $T_{IC}=95$ K. The later observation is consistent with the reported observation of new Raman peaks below

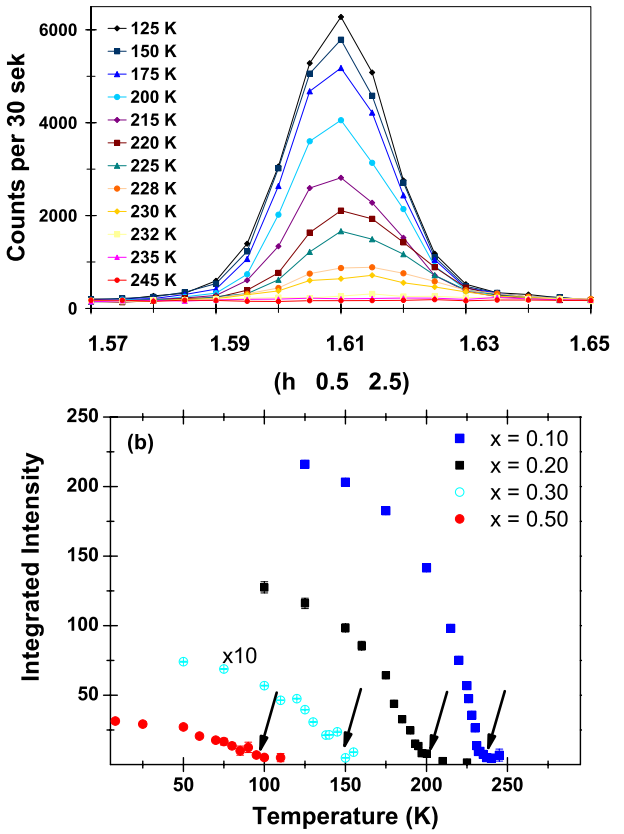

FIG. 1. (Color online) (a) The temperature dependence of the incommensurate super-lattice reflection (2-q 0.5 2.5) in $BaMn_{0.90}Zn_{0.10}F_4$ obtained by x-ray diffraction. Note that while the position of the peak stays constant, the intensity decreases with increasing temperature and vanishes above 230 K. (b) Temperature dependence of the integrated intensities of the (2-q 0.5 2.5) superlattice reflection obtained by x-ray measurements for different compositions $BaMn_{1-x}Zn_xF_4$. For $x=0.30$ the values were multiplied by 10, the weak signal is explained by the poor quality of the crystal. The general decrease in intensity of this reflection with increasing x is not quantitative as varying degrees of extinction of fundamental reflections such as the (002) between compositions prohibited its use for normalization. In general we found that the intensity of this superlattice reflection to be between 0.2% and 0.7% of the fundamental (002) reflection.

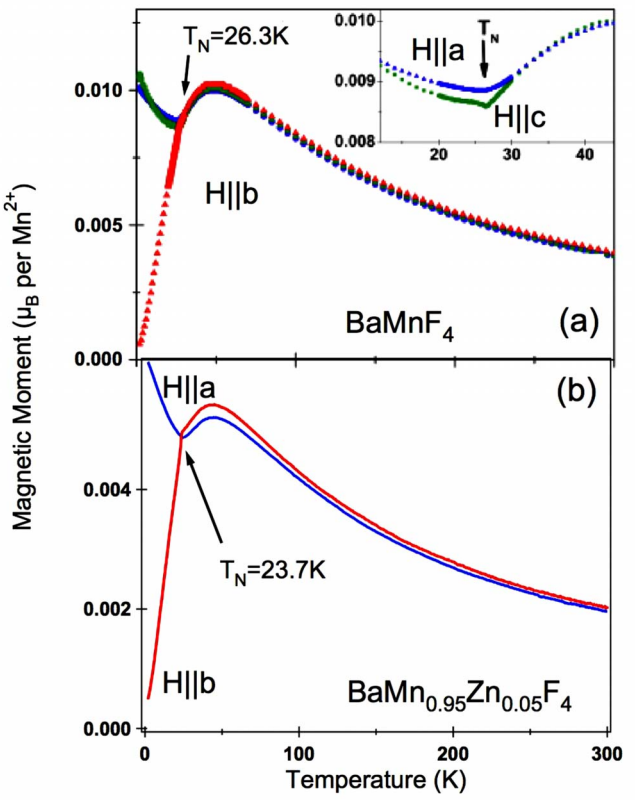

FIG. 2. (Color online) Temperature dependence of the magnetic susceptibility for (a) of $BaMnF_4$ and (b) $BaMn_{0.95}Zn_{0.05}F_4$ measured from single crystals with an applied field of 0.2 T along the principle crystallographic directions.

100 K.[24] For $x=0.75$ no super-lattice reflections were found down to 10 K. The behavior we show here of T_{IC} with increasing x is in agreement with the picture in which the mean-ionic size of the X cation is related to a lattice instability that results to the IC phase.[4,21]

B. Magnetic properties

We now turn our attention to the magnetic properties of the $BaMn_{1-x}Zn_xF_4$ solid solution. In Fig. 2(a) we show the magnetic susceptibility from $BaMnF_4$ measured from a single crystal with field applied along the a, b, and c axis. From this data it is clear that an antiferromagnetic transition takes place at $T_N=26.3$ K and that the easy axis is along b, as reported previously.[15,17] The hump in the susceptibility is interpreted as the build up of 2D spin correlations leading up to the three-dimensional spin ordering at T_N. These data on the undoped compound are used to compare the behavior of the magnetic susceptibility in the $BaMn_{1-x}Zn_xF_4$ solid solution shown in Fig. 3. In these data, measurements were either made in aligned single crystals with $H\|a$ ($x=0$, 0.05, and 0.5) or in crystals with a random orientation with respect to H. The data for the $x=0.05$ and 0.1 samples are very similar to those for the a or c axis in the undoped crystal and clearly show that T_N decreases with increasing Zn content. For the $x=0.2$ and 0.3 data sample, the sample shows a somewhat different behavior with the appearance of a peak in the susceptibility at 12.5 and 6.5 K, respectively, on top of steeply rising signal. It is reasonable to interpret this peak as the onset of an antiferromagnetic ordering, however, the precise details of the magnetic structure at this composition are still unknown. For $x=0.50$, 0.75, and 1 no anomaly in the susceptibility is found down to $T=2$ K, suggesting the absence of long-range magnetic ordering and a diamagnetic behavior. For the $x=0.5$ sample, magnetic susceptibility measured along the principle directions is essentially identical, demonstrating an isotropic behavior, while the inverse susceptibility [inset of Fig. 3(f)] follows a linear behavior down to 25 K. We speculate that a change in slope in the inverse susceptibility at 25 K may be ascribed to short-range spin correlations.

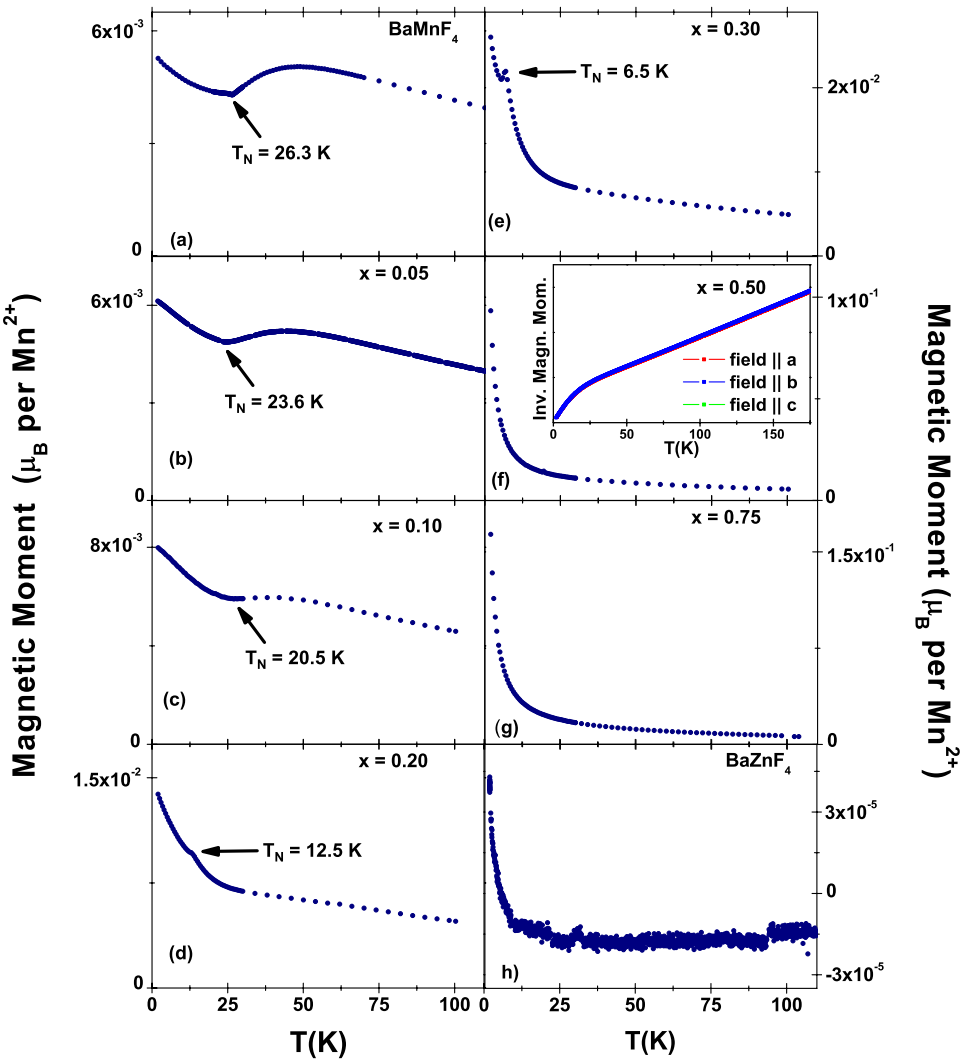

FIG. 3. (Color online) Magnetization M(t) of $BaMn_{1-x}Zn_xF_4$ single crystals in a magnetic field of $B=0.1$ T. Measurements (a), (b), and (f) were performed with a VSM, whereas the others with a SQUID. Measurements (a), (b), and (f) are measurements on oriented samples with magnetic field parallel to the crystallographic *a* axis, all other compositions have random orientation. For 50% and 75% Zn no anomaly is found down to $T=2$ K. The inverse magnetization of $BaMn_{0.5}Zn_{0.5}F_4$ with magnetic field of $B=0.1$ T along the three crystallographic axis is shown in the insert of (f). $M^{-1}(T)$ is found to be independent from the field direction and shows a paramagnetic behavior down to about 25 K. Below that temperature additional contributions exist.

IV. DISCUSSION AND CONCLUSION

The results of the structural and magnetization measurement of the $BaMn_{1-x}Zn_xF_4$ solid solution are summarized in Fig. 4. In addition to the measurements we report in this work, in Fig. 4 we also add differential scanning calorimetry (DSC) data which track the transition into the IC phase from reference.[24] The structural measurements show a linear decrease of T_{IC} with increasing x down to 50% Zn. This behavior is attributed to the decrease of the mean-ionic size of the X cation ($r_{Mn^{2+}}=80$ pm and $r_{Zn^{2+}}=74$ pm) which makes the IC phase energetically less favorable.[17] The magnetization measurements, summarized in Fig. 5, show a linear decrease of $T_N(x)$ with increasing Zn content. Indeed a linear extrapolation would indicate that T_N decreases to zero temperature at $x\sim 0.4$, consistent with the absence of magnetic ordering for sample with $x>0.3$.

The magnetism of $BaMnF_4$ can be described as a 2D Heisenberg antiferromagnet with $S=\frac{5}{2}$ with only next-nearest-neighbor interactions[16] being important. As the distances between next-nearest Mn^{2+} are 3.92 and 4.22 Å, respectively,[11] the assumption of a square lattice can be justified. In $BaMn_{1-x}Zn_xF_4$ for small Zn doping, the dilution of the magnetism is not strong enough to destroy the long-range magnetic ordering.

Randomly diluted 2D Heisenberg systems have been studied with a variety of theoretical approaches in the last decades and the percolation threshold is estimated to be $x_p^{\text{theo}}=0.407253(5)$.[26] The value of x_p^{theo} is predicted to be independent from the presence of anisotropy, as long as only nearest neighbors interactions are present.[27] The reduction rate of $T_N(x)$ as a function of the concentration of the nonmagnetic ions is described by the differential $R=-\frac{d}{dx}\left(\frac{T_N(x)}{T_N(0)}\right)$. R has been studied for various lattices and is found to be $R=\pi$ for the isotropic square-lattice 2D Heisenberg antiferromagnet and $R=1.33$ in case of the square-lattice 2D Ising antiferromagent.[28] For Heisenberg antiferromagnets with anisotropy, R is predicted to be smaller than π, which has been verified for $Mn(HCOO)_22(NH_2)_2CO$, a square-lattice weak-anisotropy 2D Heisenberg model system with $S=\frac{5}{2}$.[29]

In the case of $BaMn_{1-x}Zn_xF_4$, it is also possible to obtain x_p and R from the Zn dependence of the Nèel temperature $T_N(x)$. As shown in Fig. 5 the decrease of T_N space with increasing Zn can be described by a linear fit, giving $x_p^{\text{exp}}=0.393(4)$ and $R=2.58(9)$. These values are in good agreement with the expected values for a site-diluted square-lattice 2D Heisenberg antiferromagnet with $S=\frac{5}{2}$. The decrease of the critical spin-flop field found in $BaMn_{0.95}Zn_{0.05}F_4$ and the magnetization curves of

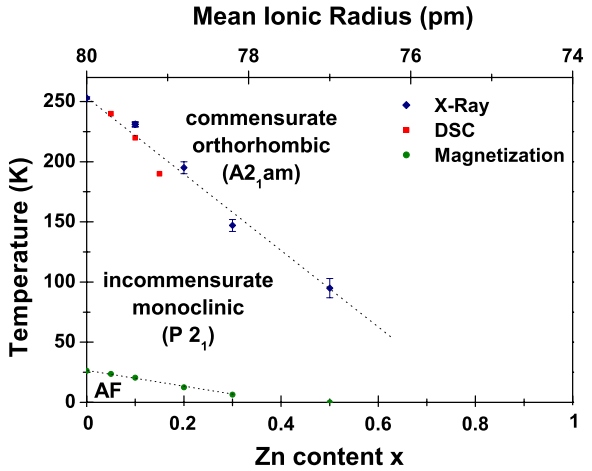

FIG. 4. (Color online) Magnetic and structural phase diagram of $BaMn_{1-x}Zn_xF_4$, compiled from x-ray diffraction and magnetization measurements. The dependence of T_{IC} and T_N on the Zn content x and the according mean-ionic radius is shown. The dashed lines are guides to the eye. For comparison, values for T_{IC} obtained with DSC measurements from Ref. 24 are shown. Values for undoped $BaMnF_4$ are shown as well for comparison (Refs. 15 and 16).

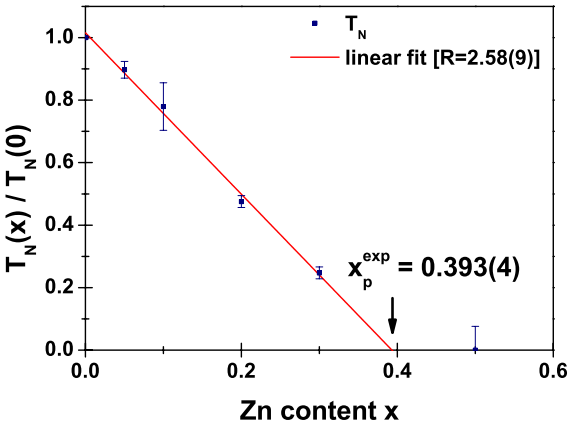

FIG. 5. (Color online) Zn dependence of the Nèel temperature $T_N(x)$ of $BaMn_{1-x}Zn_xF_4$. $T_N(0)$ is the Nèel temperature of the undoped $BaMnF_4$. By applying a linear fit, the percolation threshold x_p^{exp} and the rate R of the transition temperature change are obtained.

$BaMn_{1-x}Zn_xF_4$ for $x=0.50$ and $x=0.75$ are consistent with these findings as well.

In this work we find that the suppression of T_{IC} in $BaMn_{1-x}Zn_xF_4$ results also in a suppression of T_N as the magnetic Mn site is diluted. From bulk measurements we find evidence of an antiferromagnetic transition for x up to 0.3, while no magnetic ordering is evident in magnetization data for sample with higher Zn content. The decrease in T_N with x is described by a site-diluted square-lattice model with weak anisotropy for a Heisenberg antiferromagnet with $S=\frac{5}{2}$.

For further investigations toward materials with strong coupling between ferroelectricity and magnetism in the $BaXF_4$ family, we propose the study of $BaMn_{1-x}X_xF_4$, with X=Ni,[30] Co or Fe. In such systems a suppression of T_{IC} will be expected due to the change of the mean-ionic radius of the X cation without necessarily a suppression of T_N. As these three members of the $BaXF_4$ family have higher T_N that X=Mn (80, 70, and 60 K, respectively), it may be possible that one can achieve the formation of a material where $T_N \approx T_{IC}$. In this case, the energy scales of the ferroelastic and magnetoelastic effects would be similar with the possibility of a coupling between ferroelectric and magnetic order.

ACKNOWLEDGMENTS

The authors benefited from discussions with A. Tennant and K. Siemensmeyer. We thank R. Feyerherm, S. Landsgesell, and P. Schubert-Bischoff for assistance during the experimental work. We also thank G. Niesseron and J. Nouet for the crystal growth.

*Corresponding author. bordallo@helmholtz-berlin.de

[1] M. Fiebig, J. Phys. D **38**, R123 (2005).
[2] S.-W. Cheong and M. Mostvoy, Nat. Mater. **6**, 13 (2007).
[3] D. I. Khomskii, J. Magn. Magn. Mater. **306**, 1 (2006).
[4] C. Ederer and N. A. Spaldin, Phys. Rev. B **74**, 024102 (2006).
[5] W. Eerenstein, N. Mathur, and J. Scott, Nature (London) **442**, 759 (2006).
[6] M. Yoshimura and M. Hidaka, J. Phys. Soc. Jpn. **74**, 1181 (2005).
[7] G. Nénert and T. T. M. Palstra, J. Phys.: Condens. Matter **19**, 406213 (2007).
[8] M. Eibschütz, H. J. Guggenheim, S. H. Wemple, I. Camlibel, and M. DiDomenico, Phys. Lett. **29A**, 409 (1969).
[9] M. Eibschütz and H. Guggenheim, Solid State Commun. **6**, 737 (1968).
[10] H. Schnering and P. Bleckmann, Naturwiss. **55**, 342 (1968).
[11] E. Keve, S. Abrahams, and J. Bernstein, J. Chem. Phys. **51**, 4928 (1969).
[12] M. DiDomenico, M. Eibschütz, H. J. Guggenheim, and I. Camlibel, Solid State Commun. **7**, 1119 (1969).
[13] *Ferroelectrics and Related Substances: Inorganic Substances other than Oxides*, Landolt-Börnstein, New Series, Group III Vol. 36, Pt. B1, edited by Y. Shiozaki, E. Nakamura, and T. Mitsui (Springer-Verlag, Berlin, 2004), Chap. 26A.
[14] E. G. Villora, K. Shimamura, F. Jing, A. Medvedev, S. Takekawa, and K. Kitamura, Appl. Phys. Lett. **90**, 192909 (2007).
[15] L. Holmes, M. Eibschütz, and H. Guggenheim, Solid State Commun. **7**, 973 (1969).
[16] D. E. Cox, S. M. Shapiro, R. A. Cowley, M. Eibschütz, and H. J. Guggenheim, Phys. Rev. B **19**, 5754 (1979).
[17] J. F. Scott, Rep. Prog. Phys. **42**, 1055 (1979).
[18] P. Sciau, J. Lapasset, D. Grebille, and J. Befrar, Acta Crystallogr., Sect. B: Struct. Sci. **44**, 108 (1988).

[19] G. Samara, Solid State Commun. **21**, 167 (1977).
[20] J. Lapasset, H. N. Bordallo, R. Alamirac, and J. Nouet, Z. Kristallogr. **211**, 934 (1996).
[21] R. Almairac, H. N. Bordallo, A. Bulou, and J. Nouet, Phys. Rev. B **52**, 9370 (1995).
[22] R. Almairac, H. N. Bordallo, A. Bulou, J. Nouet, and R. Currat, Phys. Rev. B **55**, 8249 (1997).
[23] H. N. Bordallo, Ph.D. thesis, Université Montpellier II, 1995.
[24] H. N. Bordallo, R. Almairac, A. Bulou, and J. Nouet, J. Phys.: Condens. Matter **8**, 4993 (1996).
[25] *The Gnu Xtal System User's Manual*, edited by S. Hall, D. du Boulay, and R. Olthof-Hazekamp (University of Western Australia, Crawley, 2002).
[26] R. M. Ziff, Phys. Rev. Lett. **69**, 2670 (1992).
[27] K. Kato, S. Todo, K. Harada, N. Kawashima, S. Miyashita, and H. Takayama, Phys. Rev. Lett. **84**, 4204 (2000).
[28] A. McGurn, J. Phys. C **12**, 3523 (1979).
[29] K. Takeda, O. Fujita, M. Hitaka, M. Mito, T. Kawae, Y. Higuchi, H. Deguchi, Y. Muraoka, K. Zenmyo, H. Kubo, M. Tokita, and K. Yamagata, J. Phys. Soc. Jpn. **69**, 3696 (2000).
[30] J. Ferguson and H. J. Guggenheim, Phys. Rev. B **1**, 4223 (1970).